Effect of Negative Excessive Pore Pressure on the Dynamic Stability of Submerged Granular Slope

by

T. Matsushima [1], K. Date [1], T. Katagiri [2] and K. Konagai [2]

ABSTRACT

A surface slide of dense granular slope caused by an earthquake is liable to be attended by a considerable dilation. When the slope is immersed in water, the dilation causes a negative excessive pore pressure, which enhances its resistance to slide. A new conceptual model of dilative granular surface slide is presented, with the effect of pore liquid incorporated. The present approach is validated by comparing the behavior of a granular slope model, visualized by LAT (Laser-Aided Tomography), with its numerical simulation, and the development process of plastic deformation is discussed with a special concern focused on the pore liquid' s effect.

INTRODUCTION

In the seismic design of such granular structures as rockfill dams, artificial islands made of gravel and sand, it is important to evaluate the earthquake-induced permanent displacement of surface slide. However, some experimental results show that a granular assemblage has unique dynamic features which are not considered in the present seismic design codes. Tamura et al.(1) studied the dynamic behavior of rockfill dam by shaking different types of embankment models made up of the gravels of various grain size. Each model was shaken sinusoidally and the amplitude of oscillation was increased linearly with time. The surface of a model began to slide when the base acceleration exceeded a threshold. In their experiments, the threshold acceleration increased with increasing size of the grains. Konagai et al.(2) conducted dynamic failure tests of submerged embankment models made up of coarse glass particles. They visualized the particle dislocation within a slope using their original technique, LAT (Laser-Aided Tomography). In their experiments, the failure acceleration increased with increasing excitement frequency. The above-mentioned phenomena seem to have been greatly affected by a considerable dilation of the slid surface. Based on this consideration, Konagai et al.(3) have presented a conceptual model of a dilative granular surface slide. In their original model, an aggregated grains mass moves downward after being once pushed up on a grain embedded on a slip surface, and this motion triggers the entire surface failure. The effect of grain size and excitement frequency on the failure acceleration has been qualitatively explained with this model. Konagai and Matsushima(4), then, revised their original model and applied it to permanent displacement analysis of an infinite granular slope. In their revised model, the parameters for the analysis are directly related to

[1] Takashi Matsushima, Kensuke Date, Graduate Student, University of Tokyo
[2] Toshihiko Katagiri, Kazuo Konagai, Institute of Industrial Science, University of Tokyo

reliable geotechnical parameters which are obtained through some established element tests like triaxial compression tests. The slope is assumed to have an infinite extent along its surface. A one-dimensional upright soil column is then cut out of the slope. The column includes continuously-distributed plastic shear planes (1-D plastic column model), thus, allowing the column to deform continuously. The analysis of the deforming process of the column revealed that the frequency dependence of failure acceleration is greatly affected not by the surface mass, but by the shear band thickness.

When a submerged granular structure is concerned, excessive pore pressure plays an important role in its dynamic stability. When a cyclic load is applied to a loose granular slope, the slope is deformed being accompanied by a settlement, which leads to an increase of pore pressure and thus reducing the effective stress within the slope. It occasionally causes liquefaction. On the other hand, when a dense granular slope is concerned, dilation causes excessive negative pore pressure, which may enhance the effective normal stress on the sliding surface of the slope. This effect must be more pronounced as the permeability coefficient decreases.

In this study, the effect of excessive pore pressure is incorporated in the 1-D plastic column model. Permanent displacement of an infinite granular slope is then analyzed, and the contribution of excessive negative pore pressure to the dynamic stability of a granular slope is examined. Moreover, a series of dynamic failure tests of granular slope model are conducted using LAT in order to obtain the dynamic variation of excessive pore pressure during the surface slide and to compare it with the numerical result.

VISUALIZED DILATING PROCESS OF GRANULAR EMBANKMENT

Konagai et al.[3] observed the dilating process within a coarse granular slope by means of their original visualization method, Laser-Aided Tomography (LAT). In their experiments, crushed and screened glass grains (2 mm<grain<5 mm) were piled up into an isosceles shape (height = 90 mm, slope = 1:2) in a water tank full of liquid with the same refractive index as the glass. An intense laser-light sheet was then passed through the transparent model to illuminate the contours of all the particles within the optically cut cross-section. An increasing sinusoidal shake was given to the model's base. When the base acceleration exceeded a threshold, the embankment's surface began to slide. **Figs. 1(a)** and **1(b)** show the mid-cross-section of the embankment model before and after sliding. These photographs were taken at (a) and (b) in **Fig. 2**, respectively. **Fig. 2** shows the variation with base acceleration of the cross-sectional area of the

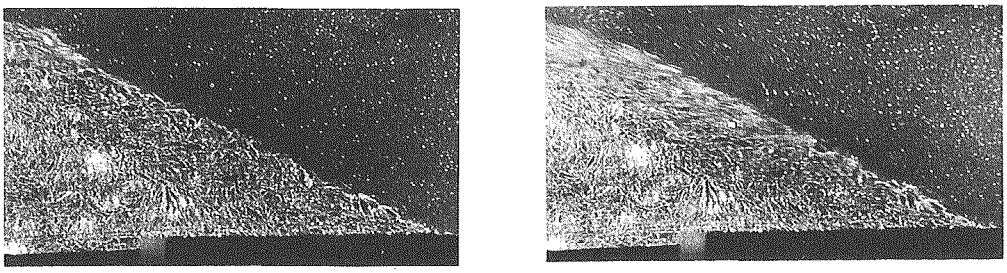

(a) before sliding (t = 5 s, acceleration=20 gal)

(b) after sliding (t= 7 s, acceleration=28 gal)

Fig. 1 Surface slide of embankment model

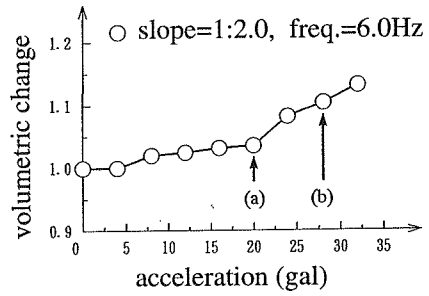

Fig. 2 Volumetric change of embankment model

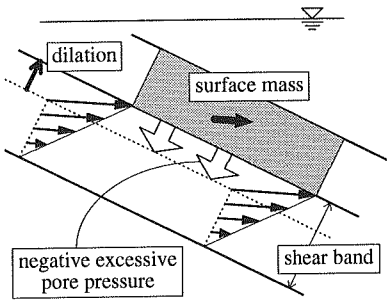

Fig. 3 Negative excessive pore pressure caused by dilation

embankment. It is obvious that the surface failure of the embankment is accompanied by considerable dilation.

When a saturated slope surface made up of densely packed fine or coarse grains begins to slide due to an earthquake, the considerable dilation may cause negative excessive pore pressure within the slope and it is worth thinking the possibility that the negative excessive pore pressure keeps plastic displacement of the slope back from being developed (**Fig. 3**). Taking this effect into account, a new conceptual model of granular surface slide is presented.

1-D PLASTIC COLUMN MODEL WITH EFFECT OF NEGATIVE EXCESSIVE PORE PRESSURE INCORPORATED

Fig. 4 shows a soil column cut out of a submerged embankment. Pore pressure p can be divided into dynamic and static terms as:

$$p = \Delta p + \rho_w g(H - z) \qquad \text{....(1)}$$

where, Δp = excessive pore pressure and $\rho_w g(H-z)$ = static water pressure.

The equations of motion governing the plastic deformation of the submerged soil column are given as:

$$\rho \cdot dz \cdot (\ddot{u}\cos\nu_d + \ddot{u}_{bottom}\cos\theta) = \rho' \cdot dz \cdot g\sin\theta - \frac{\partial F_x}{\partial z}dz$$

$$\rho \cdot dz \cdot (\ddot{u}\sin\nu_d + \ddot{u}_{bottom}\sin\theta) = -\rho' \cdot dz \cdot g\cos\theta - \frac{\partial F_z}{\partial z}dz - \frac{\partial \Delta p}{\partial z}dz \qquad \text{....(2.1), (2.2)}$$

where, $\rho' = \rho - \rho_w$

in which ρ and ρ_w are the densities of water-saturated soil column and water, respectively, u and u_{bottom} are plastic displacement of soil column and the displacement given to the base of the column, ν_d is the angle of dilation and θ is the inclination of slip surface. F_x and F_z are effective reaction force components, which satisfy the following equation as:

$$F_x = -F_z \tan\phi_{mob} \qquad \text{....(2.3)}$$

In the above eqs. (2.1)-(2.3), $\sin\nu_d$, $\sin\theta$ and $\tan\phi_{mob}$ are approximated by their angles ν_d, θ and ϕ_{mob}, and cosines of these angles approximate 1, respectively. It is also assumed the acceleration normal to the shear band is negligibly small. These assumptions lead to:

$$\rho\ddot{u} = \rho' g\theta - \frac{\partial F_x}{\partial z} - \rho\ddot{u}_{bottom}$$

$$\rho' g = -\frac{\partial F_z}{\partial z} - \frac{\partial \Delta p}{\partial z}$$

$$F_x = -F_z \phi_{mob}$$

....(3.1)-(3.3)

Darcy's law is written as:

$$\dot{w} = -\frac{k}{\rho_w g}\frac{\partial (p + \rho_w g z)}{\partial z} = -\frac{k}{\rho_w g}\frac{\partial \Delta p}{\partial z}$$

....(3.4)

It is assumed that the granular structure is completely saturated with incompressible water. Therefore the change in the flow velocity with respect to z, $\partial \dot{w} / \partial z$ is expressed in terms of the void ratio e as:

$$\frac{\partial \dot{w}}{\partial z} = -\frac{\partial e}{\partial t} \qquad \text{....(4)}$$

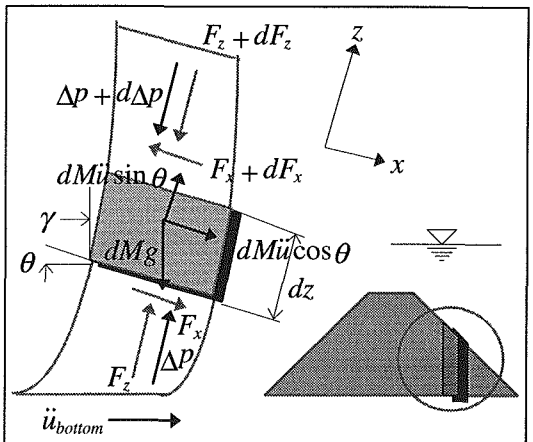

Fig. 4 Soil column cut out of a submerged embankment

During the process of plastic deformation, increasing rate of the void ratio $\partial e / \partial t$ is written as:

$$\frac{\partial e}{\partial t} = \nu_d \frac{\partial \gamma}{\partial t} \qquad \text{....(5)}$$

Differentiating eq. (3.4) with respect to z, and equating it with eq. (4) after substituting eq.(5) into eq. (4), the following equation is obtained:

$$\nu_d \frac{\partial \gamma}{\partial t} = \frac{k}{\rho_w g}\frac{\partial^2 \Delta p}{\partial z^2} \qquad \text{....(6)}$$

Eq. (3.2) is integrated with respect to z as:

$$F_z = \rho' g(H - z) - \Delta p = M' g - \Delta p \qquad \text{....(7)}$$

Differentiating eq. (3.3) with respect to z, and using eqs. (3.2) and (7), the following equation is obtained:

$$\frac{\partial F_x}{\partial z} = -\phi_{mob}\frac{\partial F_z}{\partial z} - F_z \frac{\partial \phi_{mob}}{\partial z} = \phi_{mob}\left(\rho' g + \frac{\partial \Delta p}{\partial z}\right) - (M' g - \Delta p)\frac{\partial \phi_{mob}}{\partial z} \qquad \text{....(8)}$$

Substituting eq. (8) into eq. (3.1) results in:

$$\rho\ddot{u} = \rho' g\theta - \phi_{mob}\left(\rho' g + \frac{\partial \Delta p}{\partial z}\right) + \frac{\partial \phi_{mob}}{\partial z}(M' g - \Delta p) - \rho\ddot{u}_{bottom} \qquad \text{....(9)}$$

During the shearing process of the element, the stress-dilatancy equation is approximated by the following equation[1] (saw-blades model[(5)]).

$$\phi_{mob} = \mu + \nu_d \qquad \text{....(10)}$$

In actuality dilation angle ν_d varies with shear strain γ. In the present conceptual model ν_d is assumed to satisfy the following relation[(4)].

$$\nu_d = \nu_{max} - \gamma \qquad \text{....(11)}$$

[1] Bolton[(5)] proposed the following equation instead of eq.(10) which is based on the published triaxial and plane strain data for 17 different sands.

$$\phi_{mob} = \mu + \eta\nu_d \quad (\eta = 0.8)$$

Noting that eqs.(10), (11) and $\gamma = \partial u / \partial z$, eqs.(6) and (9) are rewritten as:

$$\begin{cases} (\nu_{\max} - \dfrac{\partial u}{\partial z})\dfrac{\partial^2 u}{\partial t \partial z} = \dfrac{k}{\rho_w g}\dfrac{\partial^2 \Delta p}{\partial z^2} \\ \rho\ddot{u} = \rho' g\theta - \left(\rho' g + \dfrac{\partial \Delta p}{\partial z}\right)\left(\mu + \nu_{\max} - \dfrac{\partial u}{\partial z}\right) - \dfrac{\partial^2 u}{\partial z^2}(M' g - \Delta p) - \rho\ddot{u}_{bottom} \end{cases} \quad \text{....(12.1),(12.2)}$$

It is noted that the eq.(12.2) is valid only when the shearing is being developed. When an small element of the column is in sticking state, induced friction μ_I is smaller than μ and the element behaves like a rigid body. As soon as the absolute value of μ_I exceeds the threshold value of μ, the element is switched over to the slipping state.

In sticking state, eq. (12.2) is replaced with the following equation:

$$\frac{\partial^2 u}{\partial z \partial t} = 0 \quad \text{....(13.1)}$$

Boundary conditions are defined as follows:

(bottom)

$$\begin{cases} u = 0 \\ \dfrac{\partial \Delta p}{\partial z} = 0 \end{cases} \quad \text{....(14.1), (14.2)}$$

(top)

$$\begin{cases} \dfrac{\partial u}{\partial z} = 0 \\ \Delta p = 0 \end{cases} \quad \text{....(14.3), (14.4)}$$

NUMERICAL FORMULATION

Difference calculus is used to solve the above-mentioned equations. Eqs. (13.1) and (13.2) are rewritten as:

(slipping state)

$$\begin{cases} (\nu_{\max} - \dfrac{u_{j+1,i} - u_{j-1,i}}{2\Delta z})\dfrac{(u_{j+1,i+1} - u_{j-1,i+1} - u_{j+1,i-1} + u_{j-1,i-1})}{4\Delta z \Delta t} = \dfrac{k}{\rho_w g}\dfrac{(\Delta p_{j+1,i} - 2\Delta p_{j,i} + \Delta p_{j-1,i})}{\Delta z^2} \\ \rho\dfrac{(u_{j,i+1} - 2u_{j,i} + u_{j,i-1})}{\Delta t^2} = \rho' g\theta - \left(\rho' g + \dfrac{(\Delta p_{j+1,i} - \Delta p_{j-1,i})}{2\Delta z}\right)\left(\mu + \nu_{\max} - \dfrac{u_{j+1,i} - u_{j-1,i}}{2\Delta z}\right) \\ \qquad - \dfrac{(u_{j+1,i} - 2u_{j,i} + u_{j-1,i})}{\Delta z^2}(M' g - \Delta p_{j,i}) - \rho\ddot{u}_{bottom} \end{cases}$$

....(15.1), (15.2)

No sooner than the shear strain increment $\partial^2 u / \partial z \partial t$ changes its sign, the element sticks to the neighboring elements. Assuming that the soil column deforms monotonically in x direction, the element gets into the sticking state as soon as the following relation is satisfied:

$$u_{j,i+1} - u_{j-1,i+1} \le u_{j,i} - u_{j-1,i} \quad \text{....(16)}$$

On the sticking stage, eq. (15.2) is replaced with the following equation as:

$$u_{j,i+1} - u_{j-1,i+1} = u_{j,i} - u_{j-1,i} \quad \text{....(15.3)}$$

Eqs. (15.1), (15.2) and (15.3) are rewritten as:

$$\begin{cases} \Delta p_{j-1,i} = 2\Delta p_{j,i} - \Delta p_{j+1,i} + f_p(u_{j-1,i-1}, u_{j+1,i-1}, u_{j-1,i+1}, u_{j+1,i+1}) \\ u_{j,i+1} = f_{u,slip}(\Delta p_{j-1,i}, \Delta p_{j,i}, \Delta p_{j+1,i}, u_{j-1,i-1}, u_{j,i-1}, u_{j+1,i-1}) \\ u_{j,i+1} = f_{u,stick}(u_{j-1,i-1}, u_{j,i-1}, u_{j-1,i+1}) \end{cases} \quad \text{....(17.1)-(17.3)}$$

where,

$$\begin{cases} f_p = \dfrac{\rho_w g}{8k\Delta t}(2\nu_{mx}\Delta z - u_{j+1,i} + u_{j-1,i})(u_{j+1,i+1} - u_{j-1,i+1} - u_{j+1,i-1} + u_{j-1,i-1}) \\ f_{u,slip} = 2u_{j,i} - u_{j,i-1} + \dfrac{\Delta t^2}{\rho}\left\{\rho' g\theta - \left(\rho' g + \dfrac{(\Delta p_{j+1,i} - \Delta p_{j-1,i})}{2\Delta z}\right)\left(\mu + \nu_{\max} - \dfrac{u_{j+1,i} - u_{j-1,i}}{2\Delta z}\right)\right. \\ \qquad\qquad \left. - \dfrac{(u_{j+1,i} - 2u_{j,i} + u_{j-1,i})}{\Delta z^2}\left(M' g - \Delta p_{j,i}\right) - \rho\ddot{u}_{bottom}\right\} \\ f_{u,stick} = u_{j-1,i+1} + u_{j,i} - u_{j-1,i} \end{cases}$$

....(18.1)-(18.3)

Boundary conditions (eqs (14.1)-(14.4)) are rewritten as:

(bottom)

$$\begin{cases} u_{0,i+1} = 0 \\ \Delta p_{1,i} = \Delta p_{-1,i} \end{cases}$$ ....(19.1), (19.2)

(top)

$$\begin{cases} u_{N-1,i+1} = u_{N+1,i+1} \\ \Delta p_{N,i} = 0 \end{cases}$$ ....(19.3)-(19.4)

First of all, the plastic displacement distribution at the time t_{i+1} along the column is calculated from the bottom to the top using eq. (17.2) or (17.3), tentatively assuming that the pore-pressure distribution remains unchanged. With the displacements obtained, dynamic pore-pressure distribution Δp is obtained by the following process:

- Eq. (17.1) is rewritten at nodes 0 and 1 as:

$$\Delta p_{1,i} - \Delta p_{0,i} = f_p(u_{-1,i-1}, u_{+1,i-1}, u_{-1,i+1}, u_{+1,i+1})/2 \quad (j=0) \quad \text{....(20.1)}$$

$$\Delta p_{2,i} - 2\Delta p_{1,i} + \Delta p_{0,i} = f_p(u_{-1,i-1}, u_{+1,i-1}, u_{-1,i+1}, u_{+1,i+1}) \quad (j=1) \quad \text{....(20.2)}$$

- Adding eq. (21.1) to eq. (21.2) results in:

$$\Delta p_{2,i} - \Delta p_{1,i} = (f_p)_1 + (f_p)_0 / 2 \quad \text{....(20.3)}$$

- repeating this process, the following recurrence relation is obtained:

$$\Delta p_{J+1,i} - \Delta p_{J,i} = \sum_{j=1}^{J}(f_p)_j + (f_p)_0 / 2 \quad \text{....(20.4)}$$

- Given the boundary value, $\Delta p_{N,i} = 0$ (eq. (19.4)) at the top of the soil column, all the pore pressures $\Delta p_{j,i}$ are obtained one by one from the top to the bottom.

The values of pore pressure are then used to revise the displacement distribution. This procedure is repeated until sufficient convergence is reached.

When an element is in the slipping stage, its shear strain is being monitored, and as soon as eq. (16) is satisfied, the element gets into the sticking stage. If the whole element between two points j and j-1 were completely in sticking state, the following relation should be satisfied at both ends of the element:

$$\begin{cases} u_{j,i+1} < (f_{u,slip})_j \\ u_{j-1,i+1} < (f_{u,slip})_{j-1} \end{cases}$$ ....(21.1), (21.2)

In the actuality of the numerical calculation, however, both eqs (19.1) and (19.2) are not always satisfied simultaneously. Therefore, the element is assumed to keep sticking as far as the following relation is satisfied:

$$u_{j,i+1} + u_{j-1,i+1} < (f_{u,slip})_j + (f_{u,slip})_{j-1} \quad \text{....(22)}$$

NUMERICAL EXAMPLES

Taking the previous LAT-model size[3] as an example, a small-size (10 cm) granular column is considered. A simple half sine pulse is given to the base of the column so that the column deforms monotonically in x direction. The mechanical properties of the material are shown in **Table 1**.

Figs. 5 (a) and (b) show the displacement and pore pressure time histories of the column. The column begins to deform no sooner than the base acceleration of 220 cm/s^2 ($=\mu+\nu_{max}-\theta$) is

Table 1 Mechanical properties of the granular material

mass density ρ (t s^2/m^4)	critical angle of shear μ	maximum dilation angle ν_{max}	inclination of shear band θ	permeability coefficient k (m/s)
0.16	0.32	0.4	0.5	10^{-3}

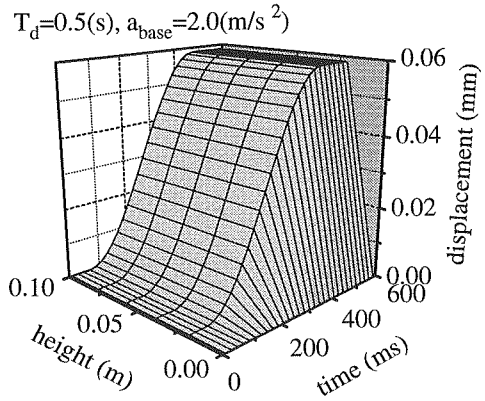

(a) displacement

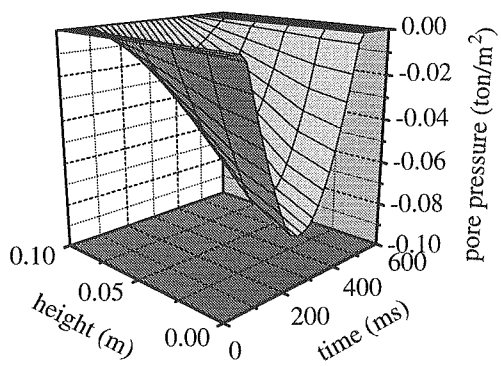

(b) negative excessive pore pressure

Fig. 5 Time histories of displacement and pore pressure distribution within column (k=10^{-3} m/s)

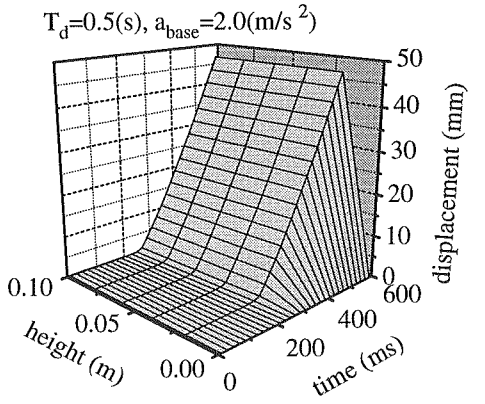

(a) displacement

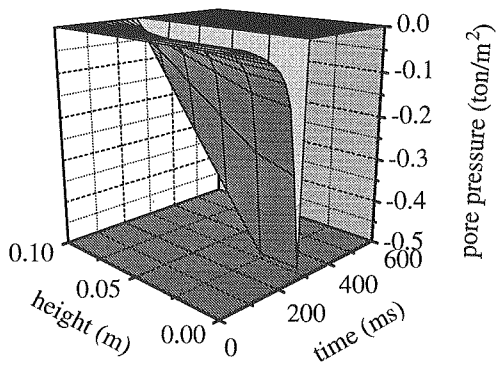

(b) negative excessive pore pressure

Fig. 6 Time histories of displacement and pore pressure distribution within column (k=10^{-2} m/s)

reached. After this value is reached, the bottom element begins to deform carrying its upper part. During this process, negative pore pressure is developed within the column (**Fig. 5(b)**). The pore pressure distribution has its bottom value at the bottom end of the column, and its minimum value is reached when the shear strain rate reaches its maximum. Beyond this point, the negative pore pressure lessens as the strain rate lessens. The elements stick to each other again at about 0.48 s, and keep sticking after that.

Figs. 6 (a) and (b) show the time histories of displacement and pore pressure within a granular column whose mechanical properties, except for the permeability coefficient, are kept unchanged. Since the permeability has been increased by 10 times, the deformation of the column develops much faster than the previous example. The rapid increase in shear deformation is accompanied by the sudden drop in excessive pore pressure within the column. The excessive negative pore pressure, however, disappears suddenly as soon as the bottom element reaches its ultimate state of shearing, because no dilation occurs beyond this point.

These two examples show the noticeable effect of pore pressure on the development of submerged surface slide. Negative excessive pore pressure provides a submerged surface with noticeable suction which enhances the resistance of the slope to slide.

LAT MODEL EXPERIMENTS OF GRANULAR SURFACE SLIDE

A series of LAT experiments were conducted to confirm the above-mentioned effect of negative pore pressure. **Fig. 7** shows the apparatus for the experiment. A model was built on a gondola hung on a steel frame fixed to a shaking table, and the gondola was shaken in a water tank. The granular slope model was made by piling up crushed and screened glass particles (2 mm< grain <5 mm) on an inclined base plate (slope=1:1.83) as shown in **Fig. 8**. The thickness of the granular layer was about 4.5 cm. The surface of the base plate is so rough that no slip took place between the plate and the particles touching it. The densities of the glass and liquid are 2.52(g/cm^3) and 0.884(g/cm^3), respectively, and the mass density of the model is about 1.86(g/cm^3). The static angle of repose of the glass grains in the liquid is 0.55(rad.). The difference of pore pressure between points A and B was measured (**Fig. 8**). An acceleration pulse shown in **Fig. 9** was applied to the base of the model.

Fig. 10 shows the middle cross-section of the slope. The opening time of the camera shutter was set at 0.5s, and the impulse was given at the mid-time of the opening. Therefore the cross section before and after excitement were superimposed on one frame of film yielding a number of pairs of bright dots. Thus the photograph provides the whole field deformation of the cross section. **Figs. 11** and **12** show the distributions of permanent displacement components normal and parallel to the slope, respectively. The motions of the particles near the toe of the slope seem to have been affected, to some extent, by the boundary "CD" in **Fig. 8**. For this reason **Fig. 10** was vertically divided in half and only the pairs of bright dots on the right half of the photograph were used to obtain the points plotted in **Figs. 11** and **12**. The curves shown in **Figs. 11** and **12** are the 4-th order polynomials, namely, the nearest paths through the plotted points. The points include the origins of the coordinates because the particles touching the base plate scarcely moved. These figures show that shear deformation of grains is localized within a certain band immediately above the base plate. The thickness of the shear band is about 0.9 cm. The dilation angle within the band approximates to 0.35.

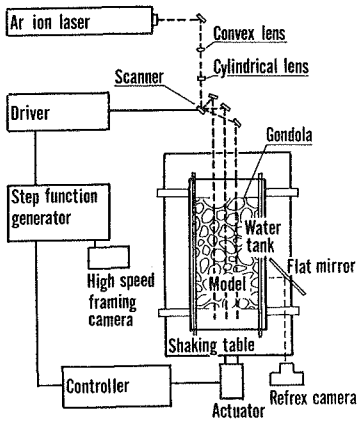

Fig. 7 Apparatus for LAT experiment

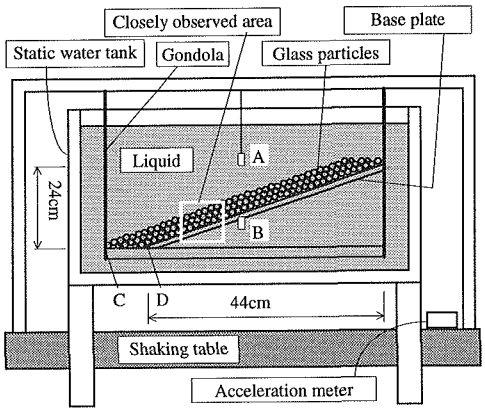

Fig. 8 Granular slope model

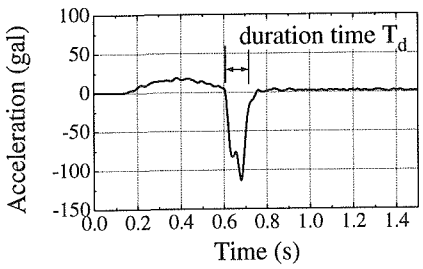

Fig. 9 An acceleration pulse applied to the model's base

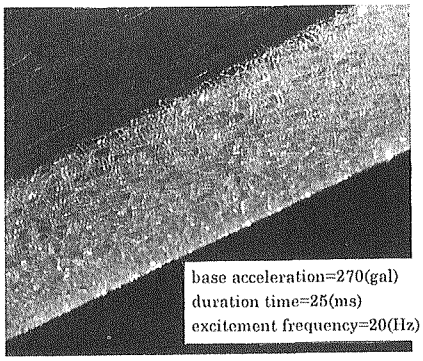

Fig. 10 Surface slide of slope model

Parameters for the analysis were shown in **Table. 2**. The thickness of each element was set at 0.9 cm reviewing the observed thickness of the shear band (**Fig. 11**). Permeability coefficient k was measured by means of the constant head permeability test. **Fig. 13** shows the variation of threshold acceleration with $1/(2T_d)$. The quantity, $1/(2T_d)$, with the dimension of frequency, is conveniently used to discuss the frequency dependence of the threshold acceleration comparing **Fig. 13** with the previous experiments[3]. In the numerical simulation, the surface mass starts slipping and never stops when the applied base acceleration exceeds a threshold. In the LAT experiment however, the boundary "CD" at the toe of the slope (**Fig. 8**) provided the surface mass with both friction and thrust. As a consequence the surface mass was kept back from slipping continuously. For this reason, the threshold acceleration in the experiment was defined as the acceleration required for the noticeable displacement of the surface mass to appear. Both curves in **Fig. 13** show that the threshold accelerations increase with increasing $1/(2T_d)$, which is consistent with the findings through the previous LAT experiments[3].

The pore pressure difference between points A and B (**Fig. 8**) is greatly affected by the flow of liquid mainly caused by the motion of the base plate. Therefore it is seemingly difficult to detect, directly from the recorded time history, the component of the excessive negative pore pressure due to the slope failure. However, the observed excessive pore pressure induced by the

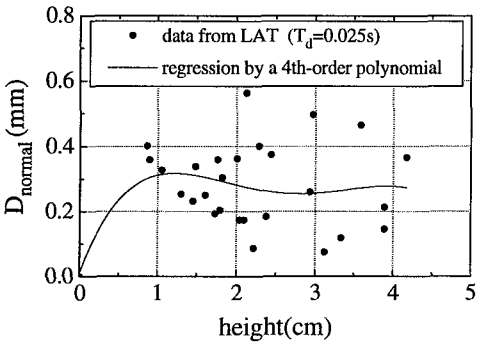

Fig. 11 Distribution of permanent displacement component normal to the slope, D_{normal}

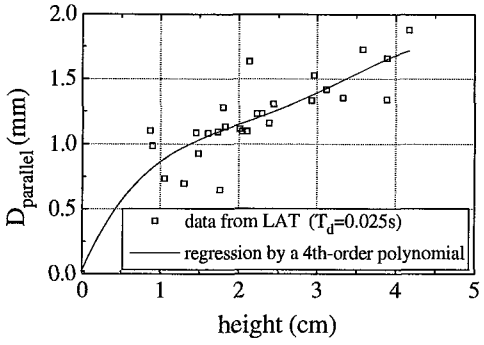

Fig. 12 Distribution of permanent displacement component parallel to the slope, $D_{parallel}$

Table. 2 Parameters used in the analysis

number of elements	5
height of column (m)	0.45
mass density (t s^2/m^4)	0.186
inclination of slope, θ	0.41
critical angle of shear, μ	0.20
maximum dilation angle, ν_{max}	0.35
permeability coefficient, k (m/s)	0.012

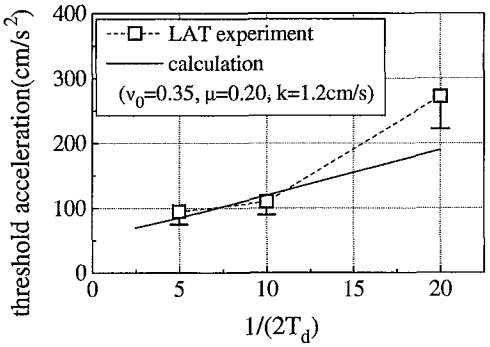

Fig. 13 Variation of failure acceleration with $1/(2T_d)$

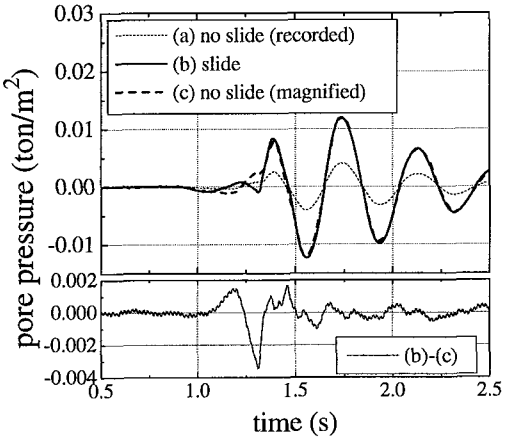

Fig. 14 Time history of pore pressure measured in the LAT experiment

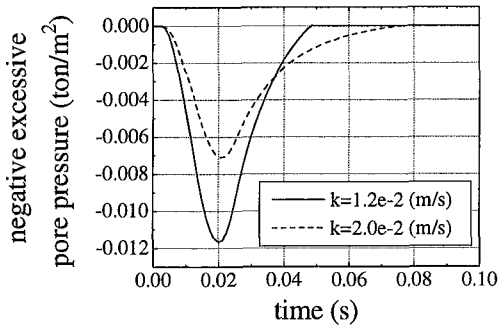

Fig. 15 Time history of calculated negative excessive pore pressure

flow has been found to be proportional to the amplitude of the base acceleration. Therefore the effect of flow of the liquid is eliminated by the following procedure:
(1) A half sine acceleration pulse a_s, which is less than the threshold, is given to the base of the model and the time history of the induced pore pressure is measured (curve (a) in **Fig. 14**).
(2) Increasing the applied impulse up to the threshold, the same process is repeated (curve (b) in **Fig. 14**).
(3) Curve (a) is then magnified by the factor a_t/a_s (curve (c) in **Fig. 14**).
(4) Subtracting curve (c) from curve (b), the effect of the flow is canceled out, thus yielding the negative pore pressure purely induced by the surface slide (curve (b)-(c) in **Fig. 14**).

Fig. 15 shows the time histories of the negative pore pressure simulated by the present model. When the permeability coefficient k is set at the measured value of 0.012m/s, the peak amplitude is about 3 times as large as the observed one. This discrepancy is possibly due to the change in the permeability coefficient during the deforming process of the slope, that is, the dilating process is attended by the increase of permeability coefficient. This phenomenon is not incorporated in the present model yet. The relation between the permeability coefficient and the void ratio, theoretically obtained by Kozeny and Carman[7], suggests that the permeability coefficient could have been possibly increased up to 0.02m/s in the experiment. The dashed line in **Fig. 15** shows the numerical result by setting k at 0.02m/s, which is closer to the observed time history.

CONCLUSIONS

Considering the effect of negative pore pressure on the dynamic behavior of a submerged dense granular slope, a new conceptual model has been presented. Permanent displacement of an infinite granular slope subjected to an acceleration pulse was analyzed by means of the present model. In the analysis, negative pore pressure induced by dilation enhanced the effective normal stress on the sliding surface of the slope. To confirm the validity of the analysis, a series of LAT experiments were conducted. Special concerns are paid to the distribution of permanent displacement within a granular slope model, the threshold acceleration required for the surface mass to slide and the negative excessive pore pressure induced within the shear band. The conclusions obtained through the study are summarized as follows:
(1) In the LAT experiment, shearing deformation of grains is localized within a certain band immediately above the base plate, which is consistent with the numerical result.
(2) It was confirmed through both the experiment and the analysis that the threshold acceleration increases with increasing $1/(2T_d)$. This tendency is consistent with the findings through the previous LAT experiments[3].
(3) The peak amplitude of the negative pore pressure simulated by the present model was about 3 times as large as the observed one. This discrepancy is possibly due to the increase of the permeability coefficient during the deforming process of the slope.

For further investigation, the change of a permeability coefficient during the dilating process should be incorporated in the present model. It is also necessary to conduct the LAT experiments by changing some important parameters including the grain size, the void ratio and the thickness of granular layer of the model.

REFERENCES

1) C. Tamura, S. Okamoto and K. Kato: Dynamic Failure Tests on Rockfill Dam Models, "Tsuchi-to-Kiso", Japan Society of Soil Mechanics and Foundation Engineering, Vol.20, No.7, 1972 (in Japanese).
2) K. Konagai, C. Tamura, P. Rangelow and T. Matsushima: Laser-Aided Tomography: A Tool for Visualization of Changes in the Fabric of Granular Assemblage, Structural Engineering/ Earthquake Engineering, Vol.9, No.3, pp.193s-201s, JSCE, 1992.
3) K. Konagai, T. Matsushima and T. Sato: Dependence on Frequency of Dynamic Inter-particle Dislocation within a Slope, Structural Engineering/ Earthquake Engineering, Vol.11, No.2, pp.93s-101s, JSCE, 1994.
4) K. Konagai and T. Matsushima: Effect of Dilation on the Dynamic Stability of Artificial Coarse Granular Slopes, 7th International Symposium on Landslides, Trondheim, Norway, June 1996 (accepted for possible publication).
5) M. D. Bolton: The Strength and Dilatancy of Sands, Geotechnique, Vol.36, No.1, pp.65-78, 1986.
6) N. Newmark: Effects of Earthquakes on Dams and Embankments, Geotechnique, Vol.15, No.2, pp.139-160, 1965.
7) S. Miwa: An Outline of Powder Technology (Funtai Kougaku Tsuuron), Nikkan Kougyou Press, 1981 (in Japanese).